Experimental and Master Equation Study of the Kinetics of OH + C_2H_2: Temperature Dependence of the Limiting High Pressure and Pressure Dependent Rate Coefficients†

Kenneth W. McKee, Mark A. Blitz, Patricia A. Cleary,‡ David R. Glowacki, Michael J. Pilling,* Paul W. Seakins, and Liming Wang§

School of Chemistry, University of Leeds, Leeds LS2 9JT, United Kingdom

Received: November 15, 2006; In Final Form: February 23, 2007

The kinetics of the reaction OH + C_2H_2 have been studied using laser flash photolysis at 248 nm to generate OH radicals and laser-induced fluorescence to monitor OH removal. An attempt was made to use the rate coefficients OH (v = 1,2) + C_2H_2 to determine the limiting high-pressure rate coefficient, k_{1a}^{∞}, over the temperature range of 195−823 K. This method is usually applicable if the reaction samples the potential energy well of the adduct, HOC_2H_2, and if intramolecular vibrational relaxation is fast. In the present case, however, the rate coefficients for loss of the vibrationally excited states by reaction with C_2H_2 also contain a substantial contribution from nonreactive vibrational relaxation, which occurs via a mechanism that does not sample the adduct potential energy well but involves, at least at low temperatures, collisions that access a shallower, longer range van der Waals well. The data were analyzed using a composite mechanism that incorporates both reactive and nonreactive energy transfer mechanisms, which allows the determination of $k_{1a}^{\infty}(T)$ for OH + C_2H_2 with satisfactory accuracy over the temperature range 195−823 K. The kinetics of the reaction OH (v = 0) + C_2H_2 were also studied in He over the range of conditions: 210−373 K and 5−760 Torr. A one-dimensional master equation (ME) analysis of the experimental data provided a further determination of $k_{1a}^{\infty}(T)$ and also $\langle\Delta E\rangle_{down}$ for He. Combining the two sets of results gives a consistent dataset for k_{1a}^{∞} and the Arrhenius parameters $A_{1a}^{\infty} = 7.3 \times 10^{-12}$ cm^3 molecule^{-1} s^{-1}and $E_{1a}^{\infty} = 5.3$ kJ mol^{-1}, with $\langle\Delta E\rangle_{down} = 150(T/300\text{ K})$ cm^{-1}. Additional experiments were conducted at room temperature in N_2 and SF_6 by laser flash photolysis with cavity ring down spectroscopy, and ME calculations were then optimized for the pressure falloff in N_2 by varying the average downward energy transfer parameter ($\langle\Delta E\rangle_{down}$). The ouput from the best fit ME was parametrized using a modified Troe expression to provide rate data for use in atmospheric modeling.

1. Introduction

The chemistry of acetylene in flames and in the atmosphere is intimately linked. Acetylene is primarily emitted to the atmosphere from road transport and biomass burning,[1] making it a clear marker for these emissions sources. It can have high concentrations in urban regions (tens of parts per billion), but its comparatively slow rate of reaction with OH limits its contribution to regional ozone formation. Its main removal mechanism from the atmosphere is reaction with OH, since it is not photolyzed or subject to rain out. Its atmospheric lifetime is ∼2−3 weeks (for a mean [OH] of ∼10^6 cm^{-3} and a rate coefficient of 7×10^{-13} cm^3 molecule^{-1} s^{-1} at 1 bar and 295 K[2]), so that it is transported over large distances. In order to include acetylene chemistry in models of the upper troposphere, rate data at temperatures down to ∼200 K are needed.

Acetylene is an important species in hydrocarbon combustion, especially under fuel rich conditions, through its involvement in soot formation mechanisms.[3] Its reaction with OH is significant, influencing radical concentrations and NO formation.[4,5]

It is clear that accurate rate parameters for OH + acetylene are required over a wide range of temperatures and pressures, for modeling both combustion and atmospheric processes.

The reaction has several possible product channels:

$$OH + C_2H_2 + M \rightarrow HOC_2H_2 + M \qquad \Delta_rH_{298} \cong -140 \text{ kJ mol}^{-1} \quad \text{(R1a)}$$

$$OH + C_2H_2 \rightarrow C_2H + H_2O \qquad \Delta_rH_{298} = 59 \text{ kJ mol}^{-1} \quad \text{(R1b)}$$

$$OH + C_2H_2 \rightarrow CH_2CO + H \qquad \Delta_rH_{298} = -95 \text{ kJ mol}^{-1} \quad \text{(R1c)}$$

$$OH + C_2H_2 \rightarrow CH_3 + CO \qquad \Delta_rH_{298} = -229 \text{ kJ mol}^{-1} \quad \text{(R1d)}$$

These products can be grouped into two distinct, low and high-temperature, regimes. At low temperatures (<1000 K), reaction 1a dominates. This is a three body reaction forming an adduct which is thermally stable at all tropospheric temperatures.[6] There is some controversy over the falloff parameters attributed to this reaction, in particular the limiting high-pressure rate coefficient for reaction 1a (k_{1a}^{∞}). The most direct measurement of k_{1a}^{∞} was conducted by Fulle et al. using a high pressure apparatus (1−130 bar He) coupled with laser flash photolysis (LFP) and saturated laser induced fluorescence (LIF) between

† Part of the special issue "James A. Miller Festschrift".

* Corresponding author. E-mail: m.j.pilling@leeds.ac.uk.

‡ Now at Department of Chemistry, University of Pennsylvania, 231 South 34th Street, Philadelphia, PA 19143. E-mail: clearypa@sas.upenn.edu.

§ Now at School of Chemistry, South China University of Technology, Guangzhou, China, 510640.

10.1021/jp067594y CCC: $37.00
Published on Web 03/31/2007

SCHEME 1

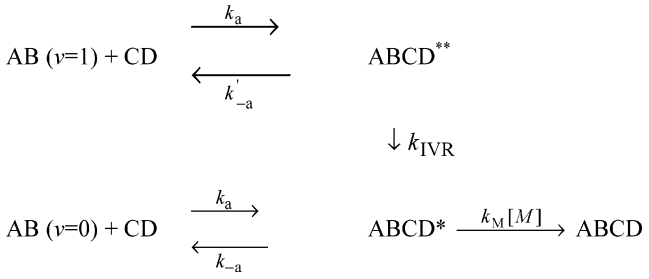

295 and 810 K.[7] They obtained $k_{1a}^{\infty} = 1.8 \times 10^{-12}$ cm^3 molecule^{-1} s^{-1} at 298 K. Their high pressure apparatus enabled the reaction to be studied near the high-pressure limit and would be expected to have returned a more reliable value than previous studies. They fitted their data with a temperature-dependent Troe broadening factor[8] to generate a 298 K falloff curve which approximately fits previous pressure-dependence studies at 298 K.[9−12] However, at 1 bar of N_2, k_{1a} is about twice that reported in the majority of previous studies.[6]

A recent IUPAC evaluation[13] recommends $k_{1a}^{\infty} = 1.0 \times 10^{-12}$ cm^3 molecule^{-1} s^{-1} at 298 K. Their analysis drew on a number of measurements at and below atmospheric pressure but was strongly influenced by the recent relative rate smog chamber experiment of Sørenson et al.,[14] who measured the rate coefficient in up to 8000 Torr of air at 296 K and obtained a value for k_{1a}^{∞} of 9.7×10^{-13} cm^3 molecule^{-1} s^{-1}. The only measurements of k_{1a} at temperatures below room temperature are those of Michael et al. from 228−413 K[10], and the IUPAC recommendation was restricted to room temperature. Senosiain et al.[15] recently reported the rate coefficient based on quantum chemistry calculations of the potential energy surface (PES), coupled with a master equation (ME) model. They found satisfactory agreement with experiment, following a slight adjustment (4.6 kJ mol^{-1}) of the calculated energy barrier for reaction 1a and obtained a non-Arrhenius form for the high-pressure limit: $k_{1a}^{\infty} = (1.80 \times 10^{-16} T^{1.34} \exp(-167\text{K}/T) + 1.00 \times 10^{-16} T^{1.62} \exp(-121\text{K}/T))$ cm^3 molecule^{-1} s^{-1}.

Measurement of k_{1a}^{∞} above room temperature, based on falloff data below atmospheric pressure, is problematic for this reaction because the reaction is far from the high-pressure limit. The use of vibrational relaxation as a proxy for the limiting high-pressure rate constant of a reaction was first proposed by Jaffer and Smith.[16] The formation of a reactive collision complex usually occurs on a long-range attractive surface, and its rate of formation, k_a, is assumed to be independent of vibrational energy. The mechanism can be schematically represented as depicted in Scheme 1. ABCD** represents the adduct prior to intramolecular vibrational relaxation (IVR), and ABCD* represents the adduct following IVR. Ergodicity is a central tenet of unimolecular reaction rate theory and appears to be valid for almost all thermal reactions. Re-dissociation of ABCD*, k_{-a}, occurs primarily to AB ($v = 0$) so that the removal rate constant derived from measurements of AB ($v = 1$) is equal to k_a which corresponds to the limiting high-pressure rate coefficient, k^{∞}. This method of directly determining k^{∞} appears to have wide validity and has been used, for example, for OH + NO,[16] NO_2,[17] and SO_2.[18] In general, as the size of the system increases, the rate of re-dissociation, k_{-a}, decreases[19] and the ergodicity assumption is more readily satisfied. Silvente et al.[20] measured the rate coefficients for OH ($v = 1,2$) + CH_3SCH_3. They found that the rate coefficient for $v = 2$ was about twice that for $v = 1$ and that both values lay below the high-pressure limit for $v = 0$. They ascribed these results to slow IVR, presumably associated with the small binding energy of the adduct (45 kJ mol^{-1}).[21] A further potential problem with the use of vibrational excitation to determine the high-pressure limit is the potential for rapid near-resonant energy transfer from AB ($v = 1$) to CD leading to a measured rate coefficient that is greater than k^{∞}. Silvente et al.[20] provide examples of this effect, which becomes more important as the size of the reaction system increases. A further potential complication arises for reactions with a barrier to adduct formation, where vibrational excitation of AB may increase k_a.

This paper describes an experimental investigation of the reaction OH + C_2H_2. The first set of experiments monitor the removal of OH ($v = 1,2$) in the presence of acetylene over the temperature range 195−823 K. Analysis of the rate data shows that energy transfer via what will be termed nonreactive vibrational energy transfer (VET), a process that does not sample the adduct potential well, is a significant contributor to the removal of vibrationally excited OH. In addition, there is a significant and identifiable contribution from the loss of vibrationally excited states via adduct formation, leading to either reaction or vibrational relaxation, depending on the pressure, from which the high-pressure limit, k_{1a}^{∞} can be determined. This assignment of k_{1a}^{∞} is shown to be reasonable by conducting a second set of experiments where the kinetics of OH ($v = 0$) + C_2H_2 was determined over a range of pressures, 5−760 Torr, and temperatures, 210−373 K, and subsequently analyzed using a ME. In agreement with other investigations,[2,14,15] this work casts doubt on the high pressure measurements of Fulle et al.[7] The low-temperature data are also used to provide expressions for $k_{1a}(p,T)$ for atmospheric applications.

2. Experimental Section

Laser Induced Fluorescence. The experimental methods are similar to those described previously;[18] thus, only the salient features are highlighted. The apparatus used to perform the ground ($v = 0$) and the vibrationally excited state ($v = 1,2$) OH kinetics were similar. The main differences were the precursors and lasers used to probe OH by LIF. An excimer laser (Lambda Physik, Compex 102), operating at 248 nm, was used as the photolysis laser, where typically 200 and <100 mJ/pulse were used for generation of OH ($v = 1,2$) and OH ($v = 0$), respectively. The hydroxyl radical was monitored by off-resonant LIF. The OH ($v = 1,2$) probe consisted of a 308 nm excimer laser (Lambda Physik, LPX 100) pumped dye laser (Lambda Physik, FL2002), which operated with the dye perterphenyl (PTP) to produce ~8 mJ/pulse. This dye laser was tuned to either 344.7 or 351.1 nm, corresponding to the Q1 branch of the $A^2\Sigma^+$ ($v = 0$) → OH $X^2\Pi$ ($v = 1$) and $A^2\Sigma^+$ ($v = 1$) → OH $X^2\Pi$ ($v = 2$), respectively, and fluorescence was collected through a 308 nm interference filter. OH ($v = 0$) was probed by (1,0) excitation using the doubled output (281.9 nm) from a Nd:YAG (Spectra Physics, GCR 140) pumped dye laser (PDL3, Rhodamine 6G) system. The subsequent fluorescence ($A^2\Sigma^+ \rightarrow X\ ^2\Pi_i$) passed through a 308 nm interference filter before capture. The OH fluorescence was detected using a photomultiplier (Electron Tubes 9813), and the resultant signal was averaged with a boxcar (SRS 232) and digitized before being stored on a PC. Little or no laser scatter was observed when detecting blue-shifted fluorescence. The PC controlled the delay generator (SRS DG535) via a general purpose interface bus (GPIB) card; the delay generator was used to fire the pump and probe lasers. Typically, the time delays were scanned over 100−200 points, with each point being the average of up to 10 samples. The lasers were fired at 5 Hz.

The gases were introduced into the reaction cell through a mixing manifold. Control of the gas flow was regulated by mass flow controllers. After the mixing manifold, the gases entered a six-way cross reaction cell designed either for high-temperature experiments with a surrounding metal block containing cartridge heaters or for subambient temperatures with a surrounding bath (~2 L) filled with methanol and CO_2(s) or silicon oil (DW-Therm, Huber) and controlled by a refrigerated immersion probe (LabPlant). The temperature was measured inside the cell by type K (high *T*) and N (low *T*) thermocouples probing near the reaction zone ensuring temperatures were known to ±3 K. The pressure in the cell was regulated by throttling the exit valve of the cell and monitored via a capacitance manometer. The total flow was >10 sccm/Torr total pressure, ensuring that the gases were swept through the cell between laser pulses. For the OH ($v = 0$) experiments, pressure and temperature were varied over the ranges 5−500 Torr and 210−373 K, respectively; for the OH ($v = 1,2$) experiments, the total pressure was ~100 Torr, and the temperature was varied over the range 195−823 K.

Absorption Spectroscopy Using CRDS. Cavity ring down spectroscopy (CRDS)[22] was employed to study the reaction in SF_6 and N_2 at room temperature, to facilitate determination of the high-pressure limit. The reaction cell was a quartz tube enclosed with two high-reflectance mirrors (reflectivity at 308 nm = 99.6%). The photolysis laser (Lambda Physik LPX 205 operating on KrF 248 nm, ~300 mJ/pulse) was expanded at right angles to the reaction cell to create a single-path absorption length of approximately 10 cm. The detection laser radiation was generated by doubling the output from a Nd:YAG 532 nm pumped dye laser (Sirah, line width ~0.017 Å) to 308.085 nm. The CRDS signal from the photomultiplier tube (PMT, Electron Tubes EMI 9813) was digitized by an oscilloscope (LeCroy LT372, 500 MHz) and transmitted to a personal computer via a GPIB interface. The signal was fitted nonlinearly to a single-exponential decay function for each laser shot. The background decay was obtained with the photolysis laser fired 20 ms after the CRDS sampling and subtracted at each decay time. Typical OH concentrations (from HNO_3 photolysis) were ~10^{11} molecule cm^{-3}, well above the sensitivity of 10^{10} molecule cm^{-3}. The typical repetition rate of photolysis was 1 Hz for a ring-down time of 0.4 μs, and the absorption path length was approximately 12 m, on the basis of the overlap between the photolysis and probe lasers.

The gases were introduced into the CRDS reaction cell through a mixing manifold. Control of the gas flow was regulated by mass flow controllers. The total flow was >2 sccm/Torr total pressure, ensuring that the gases were swept through the cell between laser pulses, and the pressure was varied over the range 50−760 Torr.

OH ($v = 0$) radicals were generated by photolyzing HNO_3 (~1×10^{14} molecule cm^{-3}) or $(CH_3)_3COOH$ (~1×10^{14} molecule cm^{-3}) at 300 K; HNO_3 was used at 373 K and $(CH_3)_3COOH$ for all experiments below 300 K. OH ($v = 1,2$) radicals were generated by photolyzing SO_2 ($(2-3) \times 10^{15}$ molecule cm^{-3}) in the presence of H_2, ($(0.5-1.5) \times 10^{17}$ molecule cm^{-1}). The method of OH ($v > 0$) generation is discussed below. All precursors were photolyzed at 248 nm, ensuring that there was no photolysis or electronic excitation of C_2H_2.

C_2H_2 (BOC) was purified by first degassing using liquid nitrogen, followed by repeated fractionation using dry ice. The purified C_2H_2 was then diluted in He. HNO_3 (Sigma Aldrich, fuming) was prepared by the addition of H_2SO_4 to the nitric acid to remove NO_2, then degassed and diluted with He. The peroxide precursors (H_2O_2 and $(CH_3)_3COOH$, Sigma Aldrich, 30% and 70%, respectively) were degassed and diluted with He. SO_2 (Air Products, 99.5%), H_2 (Air Products, 99.999), He (BOC, CP grade 99.999%), and SF_6 (99.9%) were used directly from the cylinder.

OH (v = 1,2) Generation at 248 nm. At 248 nm, acetylene has no appreciable absorption cross section.[23] However, to our knowledge, there is no suitable photolytic OH ($v = 1,2$) precursor at this wavelength. An alternative, although more complex, source is the use of highly reactive species, such as H or O^1D, which are then reacted with NO_2 or H_2 respectively, to produce vibrationally excited OH. Photolysis at 248 nm of either NO_2[24] (two-photon dissociation) or O_3 generates O^1D, which in the presence of H_2 will generate OH (v); see reaction 4. However, when acetylene is present in the system recycling can occur via

$$O + C_2H_2 \rightarrow H + HCCO \qquad \text{(R2)}$$

$$H + NO_2/O_3 \rightarrow OH\ (v) + NO/O_2 \qquad \text{(R3)}$$

This recycling obscures the removal of vibrationally excited OH by C_2H_2. In this study, $O(^1D)$ was generated by two photon dissociation of SO_2 at 248 nm:

$$SO_2 + 2h\nu_{248\ nm} \rightarrow O(^1D) + SO \qquad \text{(P1)}$$

Vibrationally excited OH was then generated by the following reaction:

$$O(^1D) + H_2 \rightarrow OH\ (v = 0-5) + H \qquad \text{(R4)}$$

Reaction 4 has been widely studied both theoretically[25,26] and experimentally[25] and is known to produce the following ratio of vibrationally excited OH:ν = 1:2:3:4; 0.26:0.29:0.28:0.17.[26] This OH source was chosen, because it can be used at 248 nm and because of the relatively slow rate of reaction of the precursors with OH:

$$OH\ (v = 1) + SO_2 = 2 \times 10^{-12}\ cm^3\ molecule^{-1}\ s^{-1} \quad \text{(ref 18)} \qquad \text{(R5)}$$

$$OH\ (v = 1) + H_2 < 1 \times 10^{-15}\ cm^3\ molecule^{-1}\ s^{-1}\ \text{(ref 27)} \qquad \text{(R6)}$$

The reaction $H + SO_2 \rightarrow OH\ (v) + SO$ does not occur at the temperatures studied here[28] and hence does not affect the removal kinetics of OH (v).

The two photon dissociation involves initial promotion of the SO_2(X) ground state to the long-lived, B Rydberg state (τ = 10−100 μs); the second photon excites SO_2 from the B to the G Rydberg state, which dissociates rapidly to products. Effenhauser[29] studied this process using photo fragment translational spectroscopy and observed nine distinct processes, corresponding to the energies required for the following processes:

$$SO_2 + 2\ h\nu_{248\ nm} \rightarrow SO\ (X^3\Sigma^-), (A^1\Delta), (B^1\Sigma^+) + O(^1D), (^3P)$$
$$\rightarrow O_2\ (X^3\Sigma^-_g) + S(^3P)$$
$$\rightarrow O_2\ (X^3\Sigma^-_g) + S(^1D)$$
$$\rightarrow O_2(a^1\Delta_g) + S(^1D)$$

Unfortunately, Effenhauser was unable to quantify the product channels because of overlapping of the time-of-flight spectra.

TABLE 1: Physical Constants Used in Master Equation Calculations[a]

species	ΔE, 0 K (kJ/mol)	rotational constants (cm^{-1})	vibrational frequencies (cm^{-1})
C_2H_2	0	1.192 05	664, 664, 766, 766, 2066, 3408, 3509
OH		19.2438	3722
TS1	6.5	0.232 16, 0.274 39, 1.369 37	198i, 108, 233, 626, 633, 667, 765, 781, 1986, 3405, 3494, 3770
C_2H_2OH	−130.7	0.320 31, 0.364 52, 2.640 58	464, 475, 566, 770, 848, 1099, 1244, 1354, 1667, 3101, 3300, 3797
TS2	10.7	0.330 65, 0.393 13, 2.061 78	2057i, 332, 807, 903, 1010, 1098, 1158, 1306, 1407, 1988, 3127, 3167

[a] Constants were derived from ab initio calculations using CBS-QCI/APNO//6-311+G(3df,2p) model chemistry.

The uncertainty of the product channel distribution and the lack of knowledge concerning the B → G transition make it difficult to quantify the concentration of $O(^1D)$ produced. An upper limit can be estimated if it is assumed that all SO_2 photolyzed produces $O(^1D)$ and that the B → G transition has a large absorption cross-section: it has been estimated that σ_{SO_2} (B → G) is $>1.8 \times 10^{-18}$ cm^2.[30] This means that ~20% of the SO_2 molecules which absorb one photon will absorb a second. Taking the measured laser power and these typical concentrations gives a maximum estimated concentration of $O(^1D)$ of 2×10^{12} molecule cm^{-3}.

Upon addition of increasing amounts of C_2H_2, fluorescence from OH ($v = 1,2$) was reduced because of the quenching of OH $A^2\Sigma^+$ and the loss of $O(^1D)$ by reaction/deactivation with C_2H_2. There does not appear to be any literature on the reaction $O(^1D) + C_2H_2$, but if one assumes it is rapid ($k > 1 \times 10^{-10}$ cm^3 $molecule^{-1}$ s^{-1}, ref 31), then there is a reduction of OH by a maximum of 50% when the highest concentrations of acetylene were added to the system. No vibrationally excited OH was found when H_2 was removed showing that no vibrationally excited OH was produced from $O(^1D) + C_2H_2$.

3. Modeling

Master Equation Calculations. Recent work on the reaction of OH with C_2H_4[32] used a ME analysis of experimental measurements to obtain a consistent set of parameters that describe the reaction rate coefficient in the falloff region for a range of temperatures. The reaction of OH + C_2H_4 is similar to OH + C_2H_2 in that a weak van der Waals complex precedes the formation of the association adduct. The reactions differ because OH + C_2H_2 has a barrier following the van der Waals complex that is higher than the energy of the reactants; for OH + C_2H_4, the barrier lies below the reactant energy. Klippenstein and co-workers[15,33] analyzed both systems using variational transition state theory, coupled with ME analysis, and argued that there is negligible stabilization in the van der Waals well. A more heuristic approach is used in the present analysis, based on inverse Laplace transformation, in which the microcanonical rate constants are linked to $k_{1a}^{\infty}(T)$. A simple Arrhenius expression, $k_{1a}^{\infty}(T) = A \exp(-E/RT)$, was used for the temperature dependence.[18,34,35]

The ME has been described previously[18,35] with recent modifications following strategies outlined in Miller and Klippenstein[36] and in Blitz et al.[28] Briefly, the population distribution for the reactants and intermediate complexes on the PES was calculated as a function of time solving a set of differential equations that describe collisional energy transfer and interconversion between species. The form of the ME used in this work is $d\mathbf{p} = \mathbf{Mp} + \mathbf{g}(t)$, where **p** is the population vector, **M** is the collision matrix that describes the rate of population transfer due to collisional energy transfer and reaction, and the vector $\mathbf{g}(t)$ represents the rate at which the individual grains are populated by the OH + HCCH association reaction. A single matrix describing collisional energy transfer in, reaction from, and formation of the adduct was generated by combining **M** and **g.** Collisional energy transfer was described using an exponential down model, parametrized with the average downward energy transferred ($\langle \Delta E \rangle_{down}$). The collision matrix was separated into 1000 discrete 20 cm^{-1} grains, diagonalized, and the eigenpairs were determined. Rate coefficients were obtained for both OH + HCCH → HOCHCH and OH + HCCH → $OCHCH_2$ by carrying out the eigenpair analysis described by Klippenstein and Miller.[37] The experimentally observed total rate of loss of OH + HCCH was obtained as the sum of the two rate coefficients given above. The procedure used to determine the best fit parameters for $k_{1a}^{\infty}(T)$ is discussed below.

Potential Energy Surface Calculations. There have been a number of calculations of the PES for OH + C_2H_2, with important early contributions from Sosa and Schlegel[38] on the addition reaction of interest here and Miller and Melius,[39] who considered a more extensive surface of relevance to combustion. More recently, Davey et al.[40] investigated the van der Waals complex OH−C_2H_2, while Senosiain et al.[15] calculated a full PES and used it to calculate rate coefficients for both the initial addition step and the subsequent reactions occurring at higher temperatures.

In the present work, the PES data for the ME simulations was obtained by carrying out geometry optimizations using density functional theory (DFT) with the hybrid B3LYP functional (in its spin unrestricted form for radicals and in its spin restricted form for closed shell species) and the 6-311+G(3df,2p) basis set. Frequency calculations were carried out on all optimized stationary point geometries, and the eigenvalues of the calculated Hessian were examined in order to verify the character of the stationary point. All first-order saddle points contain exactly one imaginary eigenvalue, which corresponds to the reaction coordinate. In addition to examining the displacement vector corresponding to the imaginary frequency of the Hessian, internal reaction coordinate (IRC) calculations were carried out on all first-order saddle points in order to verify that each saddle point connects with the relevant wells. B3LYP/6-311+G(3df,2p) geometry optimizations have been shown to achieve accurate geometries, zero-point energies, and frequencies as well as featuring a high computational efficiency; however, the calculated energies have not been shown to be sufficiently accurate for the purpose of kinetics modeling.[15] To accurately calculate the energies of the relevant stationary points for the PESs considered in this work, CBS-QCI/APNO[41] energy calculations were performed on the DFT geometries. The CBS-QCI/APNO method has been shown to give accurate energies (±4 kJ mol^{-1}) on those molecules having no more than three first row atoms that are featured in the G2 test set.[41] Details of the calculations and tabulated values of rotational constants, frequencies, and energies of the intermediates and transition states relevant to the ME modeling can be found in Table 1, all of which were obtained using Gaussian 03.[42] Optimized geometries and normal mode displacement vectors were visualized using GaussView 3.09.[42] The analysis discussed below implicitly assumes that there is little variation in the OH frequency as the reaction system moves from reactants, through

the van der Waals well and TS1 and into the reaction complex. For all species involved (all of which are given in Table 1 except for the van der Waals well, for which the OH frequency was calculated and examined), the frequency of the OH stretch changes by less than 1%.

4. Results

OH ($v = 1,2$). Laser excitation spectra of both OH ($v = 1$) and ($v = 2$) were taken under typical conditions, and simulated spectra were calculated using the LIFBASE program.[43] The calculated line positions were observed to be in excellent agreement with the experimental values.

The reaction $O^1D + H_2$, R4, has the drawback that vibrational levels up to OH ($v = 5$) are produced.[26] The fate of these high vibrational levels depends on the mechanisms of deactivation.

(i) Nonreactive VET involves a single step cascade mechanism:

$$\mathrm{OH}\ (v = x) + \mathrm{M} \rightarrow \mathrm{OH}\ (v = (x - 1)) + \mathrm{M} \qquad \text{(R7)}$$

Provided it is not close to resonant, this type of cascade mechanism is adequately described by the Shin modification of the Schwartz, Slawsky, and Herzfeld (SSH) theory which incorporates a more realistic form for the intermolecular potential than was used in the original theory.[44] For the present system, this single step cascade mechanism results in a time dependent gain term for the concentration of OH ($v = 1,2$), and the overall the reaction scheme governing the concentration of OH ($v = 1,2$) is thus

$$\mathrm{OH}\ (v = i) + \mathrm{C_2H_2} \rightarrow \mathrm{C_2H_2OH} \qquad \text{or}$$

$$\mathrm{OH}\ (v = 0) + \mathrm{C_2H_2} \qquad k_{\mathrm{R}}$$

$$\mathrm{OH}\ (v = i) + \mathrm{C_2H_2} \rightarrow \mathrm{OH}\ (v = i - 1) + \mathrm{C_2H_2} \qquad k_{\mathrm{VET}i}$$

$$\mathrm{OH}\ (v = i + 1) + \mathrm{C_2H_2} \rightarrow \mathrm{OH}\ (v = i) + \mathrm{C_2H_2} \qquad k_{\mathrm{VET}i+1}$$

where k_R is the rate constant for the process sampling the adduct well and, provided certain conditions are fulfilled, is equal to the high-pressure limit, k_{1a}^{∞}, and $k_{\mathrm{VET}i}$ and $k_{\mathrm{VET}i+1}$ are the rate constants for the nonreactive VET in OH ($v = i$) and ($v = i + 1$), respectively, $i = 1,2$

The change in concentration of OH ($v = 1,2$) is given by the general differential equation:

$$\frac{-\mathrm{d}[\mathrm{OH}(v = i)]}{\mathrm{d}t} = [\mathrm{C_2H_2}][\mathrm{OH}(v = i)](k_{\mathrm{R}} + k_{\mathrm{VET}i}) - k_{\mathrm{VET}i+1}[\mathrm{C_2H_2}][\mathrm{OH}(v = i + 1)] \qquad \text{(E1)}$$

The solution of eq 1 yields a multiexponential time dependence for OH ($v = 1,2$).[20]

(ii) Formation of the chemical adduct, HOC_2H_2, results in stabilization of the adduct or vibrational relaxation, depending on the pressure, as depicted in Scheme 1. For the lower vibrational levels, the dissociation of the chemical adduct strongly favors formation of OH ($v = 0$), and cascade relaxation is unimportant. For dissociation from higher levels, though, for example, OH ($v = 5$), a separate statistical ensemble (SSE) calculation shows that ~67% of the OH formed is in $v = 0$, with ~26% in $v = 1$ and ~6% in $v = 2$. This is still qualitatively different from nonreactive VET, with relaxation to $v = 0$ providing the major, if not the predominant, product state. Reactive and nonreactive VET could still be distinguished through an analysis of the rise times of the lower levels, although this was not feasible in the present experiments. Relaxation from these higher levels, though, does provide a minor contribution to the multiexponential character of the time dependences of OH ($v = 1,2$).

Multiexponential behavior was observed in the present system, implying that cascade was occurring. It is interesting to compare this behavior to the single-exponential loss observed for OH ($v = 1$) in the presence of SO_2,[18] where removal is wholly consistent with reactive VET. Unfortunately, there were large amounts of noise at short times in the signals obtained in the present system, so that no consistent analysis of any growth could be carried out. This scatter at short times was primarily due to spontaneous fluorescence from the SO_2 (B) Rydberg state.[23]

The early time growth data in the OH ($v = 1,2$) traces were culled and the remaining data were fitted to a single-exponential decay given by

$$[\mathrm{OH}\ (v = 1,2)]_t = [\mathrm{OH}\ (v = 1,2)]_0 \mathrm{e}^{-k_{\mathrm{obs}}t} \qquad \text{(E2)}$$

where $k_{\mathrm{obs}} = k_{\mathrm{R1total}}[\mathrm{C_2H_2}] + k_{\mathrm{other}}$, $k_{\mathrm{R1total}} = (k_{\mathrm{R}} + k_{\mathrm{VET}i})$, and k_{other} is the pseudo-first-order rate constant for loss of these states by other processes. Contributions from growth in OH ($v = 1,2$) are manifested as a decrease in the observed pseudo-first-order rate coefficient, k_{obs}.[20] To minimize this contribution from cascade, individual points were successively removed starting from $t = 0$, the decay trace was refitted, and this process was repeated until there was no increase in the fitted rate coefficient. Typical kinetic traces of OH ($v = 1$) and ($v = 2$) in the presence of C_2H_2 are shown in Figure 1, along with the best fit exponential decay.

This approach is most inaccurate when all OH removal is due to nonreactive VET. A FACSIMILE model[45] of the system, which contained the literature OH vibrational distribution, the relative rates of nonreactive VET for vibrational levels up to 5, and typical concentrations of reactants, was constructed. The relative rates of VET were assumed to conform to SSH theory:

$$k_{\mathrm{VET}_v} = k_{\mathrm{VET}_1} \times 2^{v-1} \qquad \text{(E3)}$$

where k_{VET_v} is the rate coefficient for VET from vibrational level v and k_{VET_1} is the rate coefficient for VET from $v = 1$. The model was then used to generate decay traces of OH ($v = 1,2$), and these were analyzed in exactly the same manner as the experimental traces. The analysis showed the error in the observed rate constant was at most 10−15% of the actual rate coefficient entered into the numerical model. This is consistent with the cascade analysis carried out by Silvente et al.[20] who found a discrepancy of around 5% in the exponential portion of the decay curve.

One of the difficulties in assessing the error of the pseudo-first-order fit is determining any random error associated with the culling procedure. Without knowing what the actual pseudo-first-order rate constant is, it is difficult to quantify the error. Therefore, an error of ±10%, based on the FACSIMILE analysis, was added to the pseudo-first-order rate coefficient.

The fitted rate coefficient, k_{obs}, was measured over a range of acetylene concentrations. The gradient of k_{obs} versus $[C_2H_2]$ graph is the bimolecular rate coefficient k_{R1total}. Typical plots of k_{obs} against $[C_2H_2]$ are shown in Figure 2a along with the best fit line obtained by linear regression. The intercepts of the bimolecular plots (k_{other}) were in good agreement with the relaxation/reaction rate constant in the absence of C_2H_2 due to vibrational relaxation by both SO_2 and H_2. Bimolecular rate coefficients were measured at temperatures between 195 and 810 K, and the results are shown in Table 2.

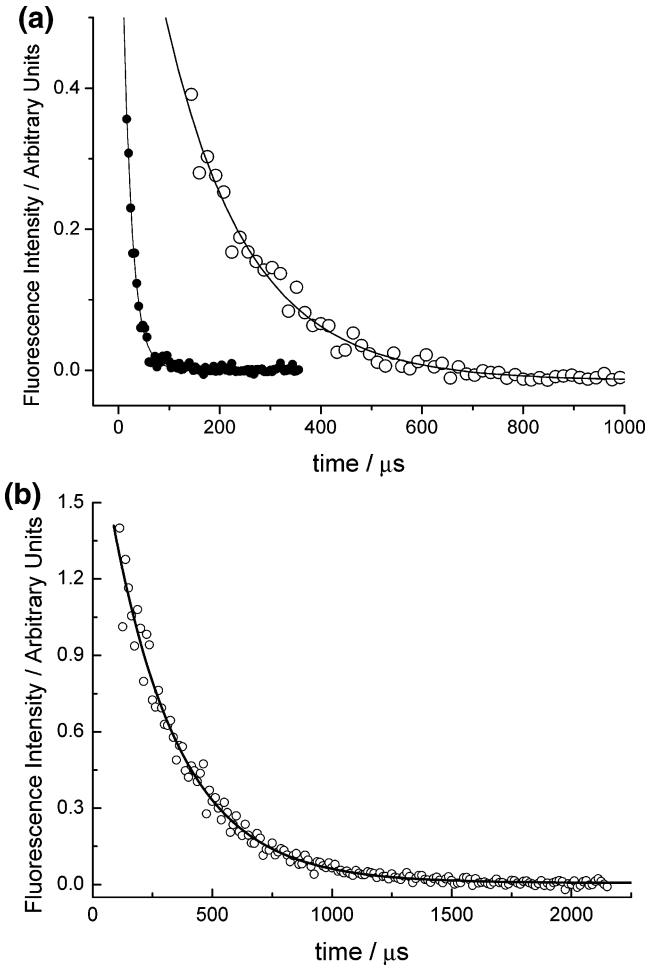

Figure 1. (a) Typical OH ($v = 1$) and OH ($v = 2$) decays. Open circles and filled circles are the measured fluorescence intensity from OH ($v = 1$) at 673 K and OH ($v = 2$) at 823 K, respectively. The lines represent the best fit exponential decay for OH ($v = 1$), $[C_2H_2] = 5.17 \times 10^{15}$ molecule cm^{-3} with $k_{obs} = (6.21 \pm 0.20) \times 10^3$ s^{-1} and for OH ($v = 2$), $[C_2H_2] = 5.97 \times 10^{15}$ molecule cm^{-3} with $k_{obs} = (5.72 \pm 0.13) \times 10^4$ s^{-1}. (b) Typical single-exponential decay of OH ($v = 0$) in the presence of C_2H_2.

OH ($v = 0$). The pressure and temperature dependence of the reaction OH ($v = 0$) + C_2H_2 was studied via FP−LIF experiments in He and N_2 and CRDS experiments in N_2 and SF_6. The photolytic OH precursors only produced OH in its ground vibrational state, so that the decay of [OH] ($v = 0$) in the presence of acetylene was observed to obey single exponential behavior (Figure 1b):

$$[\mathrm{OH}]\,(v=0) = [\mathrm{OH}]_0\,(v=0)\exp(-k_{\mathrm{obs}}t) \qquad \text{(E4)}$$

where k_{obs} is the pseudo-first-order rate coefficient and is equal to $k_{1a}[C_2H_2] + k'_{other}$. Plots of k_{obs} versus $[C_2H_2]$ were fitted to a straight line where the slope is equal to the bimolecular rate coefficient, k_{1a}. An example of such a plot is given in Figure 2b. The bimolecular rate coefficients were then determined over a range of pressures, 5−500 Torr, and temperatures, 200−373 K. The results are summarized in Tables 3 and 4.

The data from the FP−LIF experiments in He at room temperature are shown in Figure 3. The CRDS experiments in N_2 (Figure 4) fall off more rapidly with decreasing pressure than the observations of Sørenson et al. in air.[14] All other room-temperature data with N_2, air, and Ar bath gases demonstrate higher rate coefficients in the mid-pressure ranges (100−400 Torr). This work agrees better with that of Perry[11] in Ar than

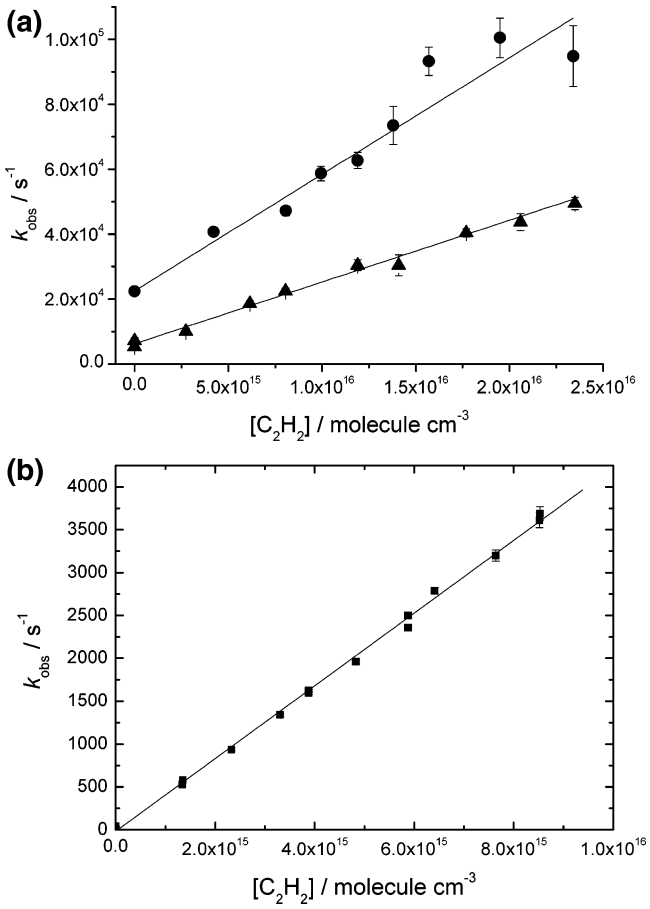

Figure 2. (a) Typical bimolecular plots for OH ($v = 1$), triangles, and OH ($v = 2$), circles, at 295 K, ∼100 Torr total pressure of He. The filled symbols are the individual pseudo-first-order rate constants, and the error bars are 1σ. The line is the linear regression and gives a bimolecular rate coefficient of $(1.90 \pm 0.20) \times 10^{-12}$ cm^3 molecule^{-1} s^{-1} and $(3.90 \pm 0.21) \times 10^{-12}$ cm^3 molecule^{-1} s^{-1} for OH ($v = 1$) and OH ($v = 2$), respectively. (b) Typical bimolecular plot for OH ($v = 0$) at 373 K, 50 Torr total pressure of He. The line regression gives a bimolecular rate coefficient of $(4.24 \pm 0.06) \times 10^{-13}$ cm^3 molecule^{-1} s^{-1}.

TABLE 2: Overall Bimolecular Rate Coefficients ($k_{R1total}$) for OH ($v = 1,2$) + C_2H_2 between 195 and 823 K[a]

T, K	$k_{R1total}$ ($v = 1$), 10^{-12} cm^3 molecule^{-1} s^{-1}	$k_{R1total}$ ($v = 2$), 10^{-12} cm^3 molecule^{-1} s^{-1}
195	2.57 ± 0.15	6.20 ± 0.54
228	2.04 ± 0.25	4.98 ± 0.32
295	1.90 ± 0.21	
298		3.59 ± 0.21
473	2.86 ± 0.32	4.26 ± 0.35
523	3.23 ± 0.28	
623	3.58 ± 0.30	
673		5.29 ± 0.40
723	3.82 ± 0.31	
823	4.10 ± 0.35	

[a] Uncertainties are two standard deviations obtained from the linear fits of the bimolecular plots.

those of Michael in Ar,[10] Sørenson in air,[14] and Wahner and Zetzsch in N_2[12] (Figure 5). However, the higher pressure results of all these groups converge to $\sim 8.2 \times 10^{-13}$ cm^3 molecule^{-1} s^{-1}, a number which agrees with the CRDS determination in SF_6. These data are in disagreement with the determinations from Fulle et al. at high pressure,[7] who observed a significantly larger high-pressure limit of 1.8×10^{-12} cm^3 molecule^{-1} s^{-1}. A full ME calculation is applied below to the data presented here to determine $k_{1a}^{\infty}(T)$ and $\langle \Delta E \rangle_{down}$.

TABLE 3: Rate Coefficients for OH ($v = 0$) + C_2H_2 at Various Temperatures and Pressures in He[a]

T, K	[He], molecule cm^{-3}	*k*, cm^3 molecule^{-1} s^{-1}
210	2.35×10^{17}	$1.40(\pm0.07) \times 10^{-13}$
210	9.40×10^{17}	$1.98(\pm0.09) \times 10^{-13}$
210	2.35×10^{18}	$2.19(\pm0.08) \times 10^{-13}$
210	4.70×10^{18}	$2.59(\pm0.09) \times 10^{-13}$
210	7.05×10^{18}	$2.85(\pm0.09) \times 10^{-13}$
210	9.40×10^{18}	$2.91(\pm0.12) \times 10^{-13}$
210	1.41×10^{19}	$3.20(\pm0.12) \times 10^{-13}$
210	1.88×10^{19}	$3.27(\pm0.11) \times 10^{-13}$
210	2.35×10^{19}	$3.22(\pm0.13) \times 10^{-13}$
233	2.12×10^{17}	$1.26(\pm0.03) \times 10^{-13}$
233	8.47×10^{17}	$2.14(\pm0.05) \times 10^{-13}$
233	2.12×10^{18}	$2.98(\pm0.08) \times 10^{-13}$
233	4.24×10^{18}	$3.46(\pm0.15) \times 10^{-13}$
233	8.47×10^{18}	$3.70(\pm0.08) \times 10^{-13}$
233	1.27×10^{19}	$3.79(\pm0.11) \times 10^{-13}$
233	1.69×10^{19}	$4.00(\pm0.09) \times 10^{-13}$
253	1.91×10^{17}	$1.50(\pm0.05) \times 10^{-13}$
253	7.63×10^{17}	$2.44(\pm0.08) \times 10^{-13}$
253	1.91×10^{18}	$3.66(\pm0.08) \times 10^{-13}$
253	3.82×10^{18}	$3.89(\pm0.12) \times 10^{-13}$
253	7.63×10^{18}	$4.68(\pm0.17) \times 10^{-13}$
253	1.14×10^{19}	$4.74(\pm0.15) \times 10^{-13}$
253	1.53×10^{19}	$4.74(\pm0.20) \times 10^{-13}$
298	1.62×10^{17}	$1.67(\pm0.05) \times 10^{-13}$
298	3.24×10^{17}	$2.18(\pm0.07) \times 10^{-13}$
298	6.48×10^{17}	$2.64(\pm0.10) \times 10^{-13}$
298	1.62×10^{18}	$3.65(\pm0.25) \times 10^{-13}$
298	3.24×10^{18}	$4.46(\pm0.27) \times 10^{-13}$
298	6.48×10^{18}	$5.48(\pm0.27) \times 10^{-13}$
298	9.72×10^{18}	$5.48(\pm0.25) \times 10^{-13}$
373	1.29×10^{17}	$1.62(\pm0.06) \times 10^{-13}$
373	2.59×10^{17}	$2.40(\pm0.13) \times 10^{-13}$
373	5.18×10^{17}	$2.93(\pm0.05) \times 10^{-13}$
373	1.29×10^{18}	$4.24(\pm0.06) \times 10^{-13}$
373	2.59×10^{18}	$5.38(\pm0.08) \times 10^{-13}$
373	5.18×10^{18}	$7.03(\pm0.13) \times 10^{-13}$
373	7.77×10^{18}	$7.12(\pm0.36) \times 10^{-13}$

[a] Uncertainties are 1σ standard deviations.

TABLE 4: Rate Coefficients for OH ($v = 0$) + C_2H_2 at Various Temperatures and Pressures in N_2 and SF_6[a]

T, K	M	[M], molecule cm^{-3}	*k*, cm^3 molecule^{-1} s^{-1}
298	N_2	1.59×10^{18}	$4.58(\pm0.35) \times 10^{-13}$
298	N_2	1.78×10^{18}	$3.77(\pm0.17) \times 10^{-13}$
298	N_2	5.44×10^{18}	$5.76(\pm0.22) \times 10^{-13}$
298	N_2	6.64×10^{18}	$6.07(\pm0.44) \times 10^{-13}$
298	N_2	8.72×10^{18}	$7.19(\pm0.53) \times 10^{-13}$
298	N_2	1.24×10^{19}	$7.15(\pm0.24) \times 10^{-13}$
298	N_2	1.57×10^{19}	$7.28(\pm0.12) \times 10^{-13}$
298	N_2	1.93×10^{19}	$8.57(\pm0.23) \times 10^{-13}$
298	SF_6	2.44×10^{19}	$7.98(\pm0.34) \times 10^{-13}$

[a] Uncertainties are 1σ standard deviations.

5. Discussion

Interpretation of the Results for OH ($v = 1,2$). The results from the experiments show two distinct temperature regimes for the rate coefficients for the removal of OH ($v = 1,2$) by acetylene (Figure 6), increasing with increasing temperature above ~300 K and increasing with decreasing temperature below ~300 K. The trend in the high-temperature regime is consistent with the barrier which has been observed previously[6] for k_{1a}^{∞}. However, reactive VET explains neither the behavior at low temperatures nor the higher rate coefficient for OH ($v = 2$). This behavior suggests that nonreactive V → T,R,V is occurring, possibly as well as reactive VET.

Schwartz, Slawsky, and Herzfeld (SSH) developed a model for vibration to translation energy transfer on a repulsive potential and showed that the rate coefficient increases with temperature according to the relationship $\ln k \propto 1/T^{1/3}$.[46] The model was extended by Shin to include an attractive component to the potential and showed that an inverse temperature dependence of the rate coefficient occurs at low temperature, where $\ln k \propto 1/T^2$.[44,46−48] Shin based his analysis on dipole−dipole or dipole−quadrupole interactions and invoked his model to explain the anomalous temperature dependence of VET for HF with several collider molecules (DF, HF, and CO_2 among others). The probability for VET was seen to go through a minimum, similarly to the present OH/acetylene system, between 300 and 700 K. Dipole−dipole (and dipole−quadrupole) interactions of the order of 15 kJ mol^{-1} were found to have a significant effect on the probability of vibrational relaxation, at temperatures as high as 500 K.

Davey et al.[40] calculated the PES in order to investigate the nature of the van der Waals complex in OH−C_2H_2. They found an equilibrium geometry at a T-shaped configuration, with the H of OH directed toward the acetylene triple bond, in agreement with the earlier work of Sosa and Schlegel.[38] There are two complexes, depending on the orientation of the unpaired electron in OH to the plane of the complex, for which Davey et al. obtained dissociation energies, D_e of 13.5 and 11.8 kJ mol^{-1}.

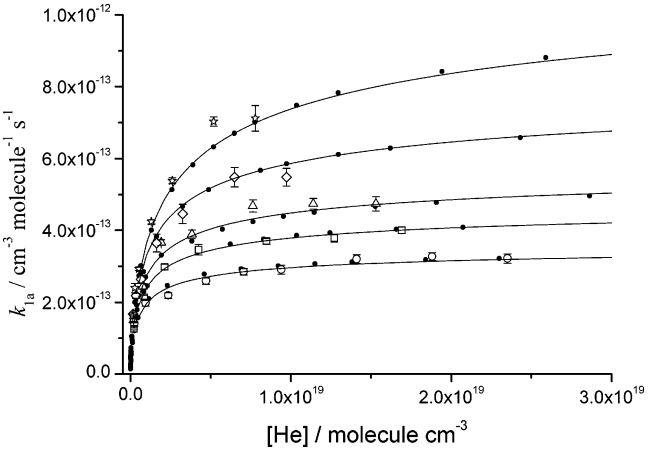

Figure 3. Bimolecular rate constants, k_{R1a}, for OH ($v = 0$) + C_2H_2 at 210 (○), 233(□), 253(△), 298(◇) and 373 K (☆) in He. Also included are the ME fits to this dataset (●) and a modified Troe fit to the ME data, solid lines; see text for details.

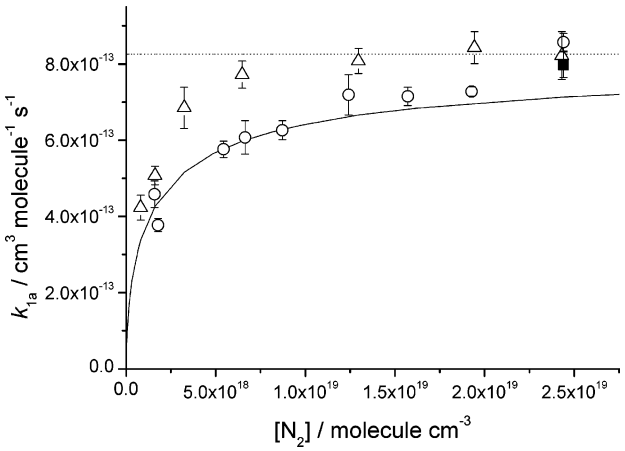

Figure 4. Bimolecular rate constants, k_{1a}, versus total pressure, *M*, for OH ($v = 0$) + C_2H_2 at 298 K: ○ = this study using CRDS and N_2 buffer gas, ■ = this study using CRDS and SF_6 buffer gas, and △ = Sorenson et al.[14] using air. The solid line is our best fit ME at 298 K using N_2 buffer gas ($\Delta E_{down} = 250$ cm^{-1}); see text. The dotted line is the high-pressure limit, k_{1a}^{∞}.

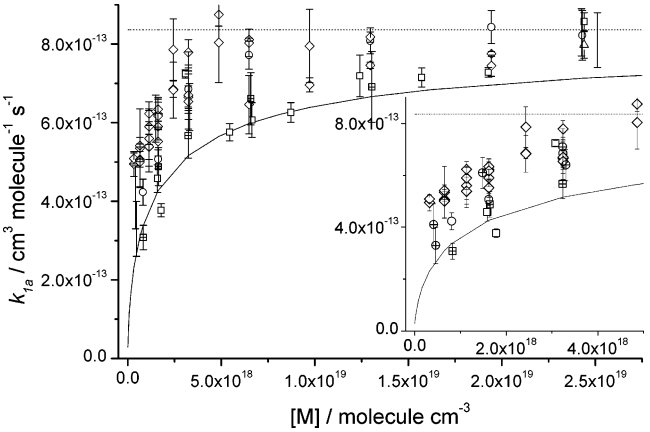

Figure 5. Bimolecular rate constants, k_{1a}, versus total pressure, M, for OH ($v = 0$) + C_2H_2 at 298 K: □ = this study using CRDS and N_2 buffer gas; △ = this study using CRDS and SF_6 buffer gas; ○ = Sorenson et al.[14] using air; ◇ = Michael et al.[10] using Ar buffer gas; ⊞ = Perry et al.[11] using Ar buffer gas and ⊕ Wahner et al.[12] using N_2 buffer gas. The solid line is our best fit ME at 298 K using N_2 buffer gas ($\Delta E_{down} = 250$ cm^{-1}); see text. The dotted line is the high-pressure limit, k_{1a}^{∞}. Inset shows the plot at low pressures where the data of Michael et al.[10] is significantly higher than our best fit ME.

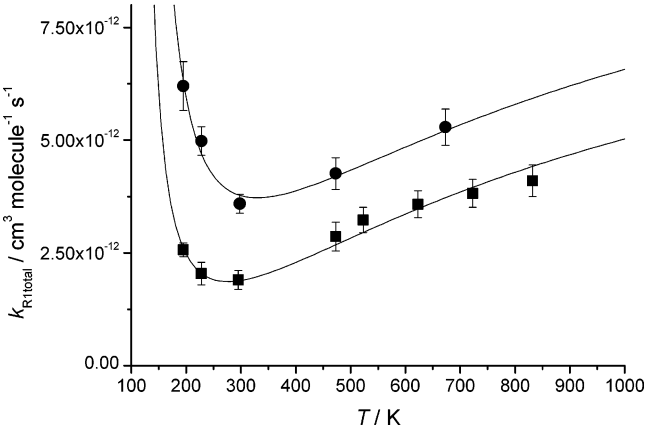

Figure 6. Fit of all relaxation processes for both OH ($v = 1$) and OH ($v = 2$). Squares are OH ($v = 1$) + C_2H_2, and circles are OH ($v = 2$) + C_2H_2. The solid line is the best fit to the data using eq E6.

They also found shallower wells at other configurations. Senosiain et al. also found that the most stable complex is T-shaped, with a dissociation energy D_0 of 8.4 kJ mol^{-1} and another asymmetric complex with a dissociation energy of 3.8 kJ mol^{-1}. In the calculations reported in this paper, the van der Waals complex was asymmetric, with $D_0 = 7.7$ kJ mol^{-1}; since its characterization was not central to the work reported here, the characteristic of other possible configurations was not investigated. Davey et al.[40] also investigated the OH/acetylene van der Waals complex experimentally and concluded that the complex is π-type hydrogen bonded with the well depth at the T-shaped minimum equal to or less than 11.4 kJ mol^{-1}. It is appropriate, therefore, to consider a nonreactive VET mechanism in which energy transfer collisions access the van der Waals well, and to utilize the theoretical framework provided by Shin.[44,46−48]

Further support for a vibration to translation energy transfer mechanism is provided by the higher rate coefficient for OH ($v = 2$). Standard SSH theory treats all vibrations as harmonic oscillators, and the rate of VET is simply doubled for each increment in the vibrational quantum number; see eq 3. However, anharmonicity reduces the vibrational energy spacing with increasing v, so that for pure V → T energy transfer, for example, between a diatomic molecule and an atom, the rate coefficient increases more rapidly with v than predicted by the SSH theory. The behavior can be more complex for energy transfer between molecules, where V → V energy transfer can also occur, reducing the amount of energy transferred to translation and so increasing the rate coefficient. Resonant energy transfer, where the energy transferred to translation is small, shows specific behavior that is not well-described by the SSH−Shin model, but Table 5 shows that there are no close resonances between OH and C_2H_2. The energy transferred to translation is minimized if the C−H stretches are excited in a V → T,V process, with the energy so transferred being reduced for OH ($v = 2$). VET from OH has been reported by Dodd et al.[49] (OH + CO_2 and O_2, where the energy transferred to translation is much higher than in the current case) and Silvente et al.[20] Empirically, the relationship between quantum number for vibration and the rate coefficient for VET can be represented by

TABLE 5: Vibrational Frequencies for OH and C_2H_2[a]

molecule	mode	vibrational frequency, cm^{-1}
OH	OH stretch	3735
C_2H_2 (υ_1)	CH stretch	3374
C_2H_2 (υ_3)	CH stretch	3289
C_2H_2 (υ_2)	CC stretch	1974
C_2H_2 (υ_5)	CH bend	730
C_2H_2 (υ_4)	CH bend	612

[a] Acetylene frequencies are taken from ref 56. OH data are from ref 57. The OH data are calculated from the differences in the energies of the vibrational levels, i.e., they incorporate anharmonicity. The acetylene data refer to the vibrational frequencies. Vibrational energy spacing in hydroxyl are OH ($v = 1 \rightarrow 0$) = 3570 cm^{-1} and OH ($v = 2 \rightarrow 1$) =3405 cm^{-1}

$$k \propto n^{\nu-1} \qquad \text{(E5)}$$

where ν is the vibrational quantum number and n is dependent on the system. For a harmonic oscillator, $n = 2$, but it would be expected to be greater than 2 for non-resonant transfer from an anharmonic oscillator.

To summarize, it is proposed that the nonreactive VET for OH ($v = 1,2$) by C_2H_2 has two contributions. At the lowest temperature, energy transfer is strongly influenced by the van der Waals well, and the rate coefficient shows a negative temperature dependence. At higher temperatures, the thermal energy becomes comparable to the well depth of the van der Waals complex, VET becomes more influenced by the repulsive interaction, and the rate coefficient for VET starts to increase. At these higher temperatures, loss of OH ($v = 1,2$) by formation of the adduct HOC_2H_2 must also be considered. Provided IVR is rapid, then the rate coefficient for this process, k_R (R1a), is equal to k_{1a}^{∞}. The analysis of Senosiain et al.[15] returns rate coefficients at these higher temperatures that are comparable with those measured for OH ($v = 1$), while the measurements of Fulle et al. are significantly higher. Figure 7 shows a comparison between k_{VET} ($v = 1$) and their k_{1a}^{∞}. It is appropriate, therefore, to analyze the data in a manner that accommodates all three mechanisms, by incorporating three distinct temperature dependences and an increase of the rate coefficient for non-reactive VET with vibrational quantum number. An appropriate form for the rate coefficient is

$$k_{\mathrm{VET}_v} = B\left[\exp\left\{-\frac{C}{T^{1/3}} + \frac{D}{T^2}\right\}\right] n^{\nu-1} + A\exp\left\{-\frac{E}{RT}\right\} \qquad \text{(E6)}$$

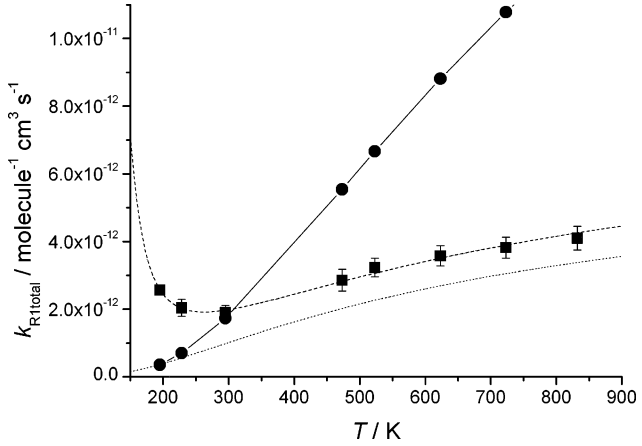

Figure 7. Plots of the $k_{R1total}$ OH ($v = 1$) data versus T, squares, the best fit to this data, dashed line, and the k_{1a}^{∞} data, dotted line, which was obtained from the A and E parameters of eq E6; see text for details. Also included are the values for k_{1a}^{∞} obtained from high-pressure measurements by Fulle et al.,[7] circles and bold line.

TABLE 6: Parameters Determined by Fitting the Data in Table 2 to Eq 6[a]

parameter	fitted
B	$(4 \pm 6) \times 10^{-12}$ cm^3 molecule^{-1} s^{-1}
C	15 ± 14 K$^{1/3}$
D	$(7.6 \pm 3.0) \times 10^4$ K^2
n	2.79 ± 0.43
A ($A_{1a}^{¥}$)	$(6.7 \pm 1.9) \times 10^{-12}$ cm^3 molecule^{-1} s^{-1}
E ($E_{1a}^{¥}$)	4700 ± 1600 J mol^{-1}

[a] Uncertainties are two standard deviations.

where k_{VET_v} is the overall bimolecular rate coefficient for loss of OH in ($v = 1,2$), A, B, C, D, and E are parameters to be determined by fitting, with $A = A_{1a}^{\infty}$, the A factor for the high-pressure limit for reaction R1a. The parameter n describes the enhancement of the rate coefficient for nonreactive VET with increasing vibrational quantum number (eq 5). For a harmonic oscillator, $n = 2$, but it was also fitted in the following analysis. The first (bracketed) term on the right-hand side of eq 6, describes nonreactive VET and is essentially a parametrized form of the extended SSH theory developed by Shin.[44,48] The second term corresponds to the high-pressure limiting rate coefficient for reaction R1a, provided IVR is fast.

Equation 6 was used to fit both the $v = 1$ and the $v = 2$ data in Table 2 simultaneously using two independent variables, T and v, using a weighting proportional to the square of the reciprocal uncertainty in k_{VET}. A nonlinear least-squares fitting routine was used to locate the best-fit parameters. The resulting fit is shown in Figure 6, and the returned parameters and uncertainties are given in Table 6.

From Figure 6, it can be seen that eq 6 provides an excellent fit to the data. The nonreactive VET parameter n is greater than 2, which is expected from the anharmonicity and the decrease in the energy transferred to translation and the non-resonant nature of the VET. Table 5 shows that no vibrations or combinations in C_2H_2 lie within 100 cm^{-1} of the OH stretches. The interpretation of the nonreactive VET B, C, and D parameters in terms of the fundamental properties of the system is beyond the scope of this analysis; indeed, the uncertainties in the parameters that are returned are substantial and obviate such an analysis. It is, though, of interest to compare the present system to HCl self-relaxation where the minimum in the rate coefficient is located at a similar temperature for a dimer well depth equal to 8.8 kJ mol^{-1}.[46,50]

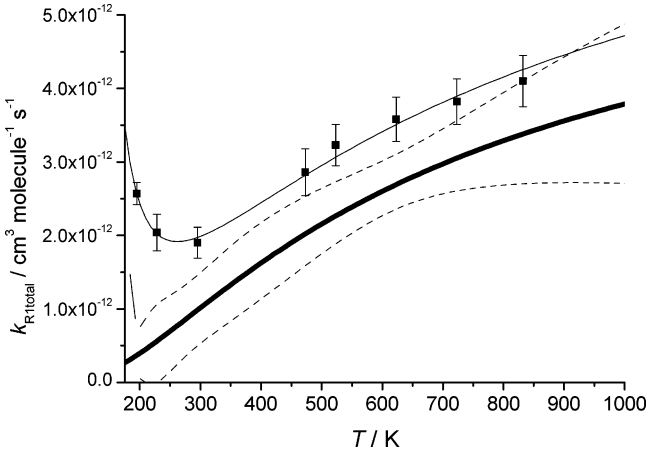

Figure 8. Plot of the $k_{R1total}$ OH ($v = 1$) data versus T, squares, together with the best fit to the data using eq E6. Also included in the plot is k_{1a}^{∞}, bold line, which is obtained from parameters A and E in eq E6. The dashed lines are the 95% confidence limits for k_{1a}^{∞}.

The main target of this analysis is $k_{1a}^{\infty}(T)$, for which the uncertainties are smaller than for nonreactive VET (Table 6). Figure 8 shows a plot of the measured rate coefficients for OH ($v = 1$) together with the best fit for the overall rate coefficient and also the fitted rate coefficient for reactive VET. The uncertainty ranges are also given. The plot shows that $k_{1a}^{\infty}(T)$ is quite well-defined, especially at high temperatures; the uncertainty returned from the confidence limits obtained from the full co-variance matrix is 88% at 200 K, 47% at 300 K, and 14% at 700 K. It is not until ~350 K that reactive VET contributes more than 50% of the total rate of removal; below room temperature, k_{VET} is a poor approximation of k_{R1a}^{∞}. The success of the fit of a limited dataset to an expression including six variable parameters derives from the observation of both positive and negative temperature-dependent regimes, the dependence of nonreactive VET on v, and the transition from low temperatures, where reactive VET is unimportant, to high temperatures, where it is.

Interpretation of the Results for OH ($v = 0$). As discussed in the introduction, the investigation of the pressure dependence of k_{1a} for OH ($v = 0$) was conducted because of the lack of data for this reaction below room temperature and the importance of this temperature regime for the upper troposphere. In addition, the reaction is closer to the high-pressure limit at 1 bar in this temperature regime, so that k_{1a}^{∞} can be more reliably obtained by extrapolation, thus, contributing to the overall determination of this quantity at temperatures where the analysis of the $v = 1,2$ kinetics is least reliable.

The approach used in the ME analysis was outlined above. Figure 9a shows the portion of the PES relevant to the ME analysis. We note that all calculated energies and constants are in good agreement with the results of Senosiain et al.[15] In order to solve the ME and model the experimental temperature-dependent falloff curves for OH + HCCH, the collision matrix was calculated by treating a single well (HOCHCH) with a bimolecular source term, and a single exit channel to $OCHCH_2$ via TS2, which is the only energetically available channel at low temperatures. According to Senosiain et al.,[15] at pressures higher than 1 atm, the only well in which significant stabilization occurs is HOCHCH. At atmospheric pressure, the decomposition of HOCHCH to H + ketene and CO + CH_3 can compete with its stabilization. The flux minimum in this reaction path occurs at TS2. In our ME simulations, TS2 thereby effectively represents the sum of these two possible decomposition chan-

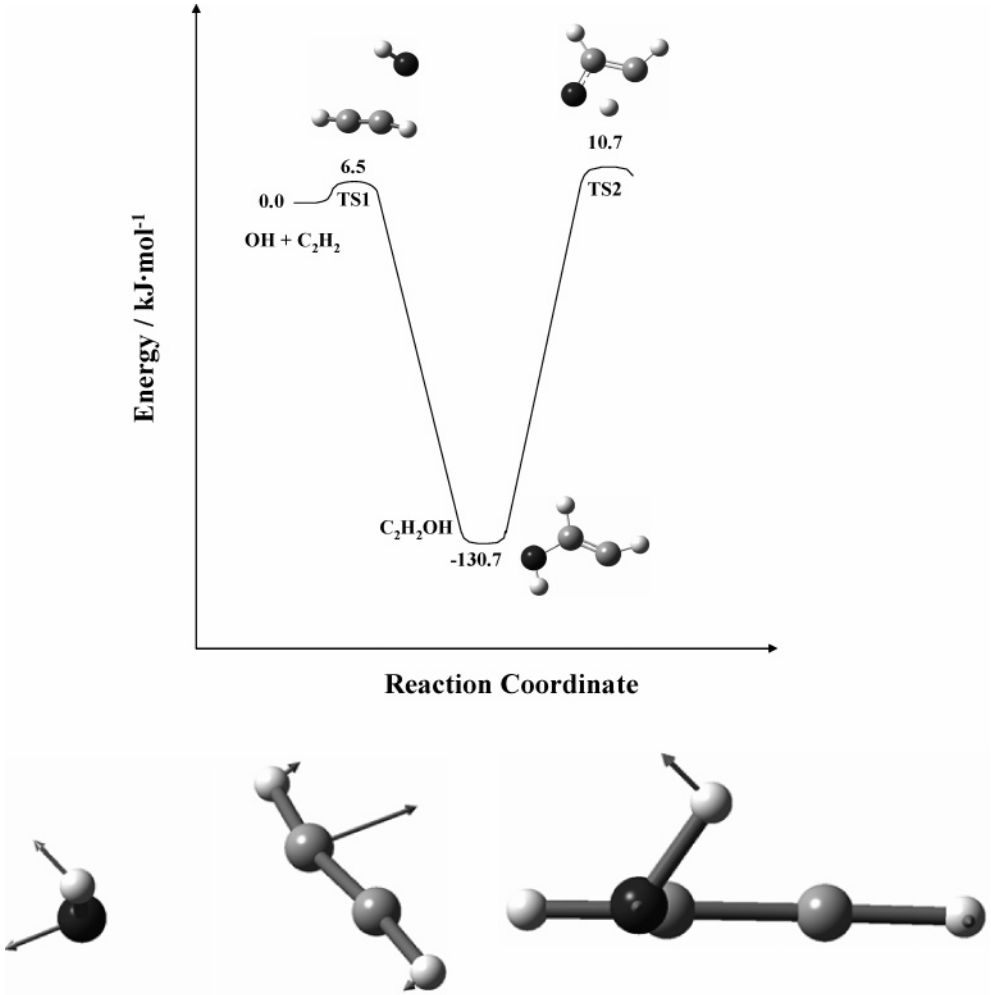

Figure 9. (a) PES for OH + C_2H_2 at the CBS-QCI/APNO//6-311+G(3df,2p) model chemistry. (b**)** Figures present two views of the displacement vectors for the normal mode that has the imaginary frequency in TS1. The above displacement vectors depict OH rotation in TS1 but do not suggest vibration of the O−H bond.

nels. Senosiain et al.[15] present a more complete PES, including the intermediates and channels following TS2. For our purposes, the aim is simply to incorporate these channels into the ME analysis to assess their contribution to the measured rate coefficient as a function of pressure and temperature. Senosiain et al. showed that the abstraction channel occurs across a significantly higher barrier and does not contribute significantly under our conditions.

The microcanonical rate coefficients for dissociation of the adduct to regenerate the reactants were determined from $k_{1a}^{\infty}(T)$ by inverse Laplace transformation (ILT),[34] and the microcanonical rates of forming the adduct were obtained by detailed balance. This approach was used because of the complex nature of the surface up to and including TS1, which obviates facile direct calculation of $k(E)$. The ILT technique provides a mechanism whereby $k(E)$ can be linked directly to the experimental rate data. The microcanonical rate coefficients for the reaction across TS2 were obtained from the PES parameters. The vibrational frequencies and rotational constants for OH, C_2H_2, HOC_2H_2, and TS2 are shown in Table 1; the calculated parameters for TS1 are also included, although they were not directly used in the calculation.

The rate coefficients, $k_{1a}(T,p)$ were determined from the ME using the Arrhenius parameters for $k_{1a}^{\infty}(T)$, that is, A and E, as variable parameters together with $\langle\Delta E\rangle_{\text{down}}$. k_{1a} was determined for each of the 37 conditions of helium pressure and temperature used experimentally and repeated over a three-dimensional grid of A, E, and $\langle\Delta E\rangle_{\text{down}}$ values: a total of 10 360 solutions of the ME. A measure of χ^2 was determined from S^2, the sum of the squares of the differences of the calculated and measured rate coefficients and the position of the minimum on the hypersurface determined. Two models were used for $\langle\Delta E\rangle_{\text{down}}$, one with $\langle\Delta E\rangle_{\text{down}}$ temperature independent, the other varying linearly with temperature. The latter model showed a lower value for the minimum χ^2. Figure 10 shows a contour plot of χ^2 versus A and E, for $\langle\Delta E\rangle_{\text{down}} = 150(T/300\text{ K})\text{ cm}^{-1}$, which is the optimal expression. The minimum is well-defined and gives $A = 7.1 \times 10^{-12}$ cm^3 molecule^{-1} s^{-1} and $E = 5.4$ kJ mol^{-1}. Rate coefficients calculated from the ME using these best fit parameters are shown in Figure 3.

The ME analysis included calculation of the overall rate coefficient for the reaction channels accessed via TS2. Under the conditions studied experimentally, the fractional contribution to the overall rate coefficient from these channels was small (e.g., 3% at 10 Torr and 0.7% at 100 Torr, at 298 K). The channel becomes more significant at lower pressures (32% at 0.1 Torr and 9% at 1 Torr, at 298 K). Senosiain et al.[15] concluded that formation of H + ketene is the major channel, for that part of the flux that proceeds over TS2, at atmospheric pressure and temperatures below 2100 K.

Figure 3 compares the experimental values with those determined from the ME using the optimal parameter set. Troe

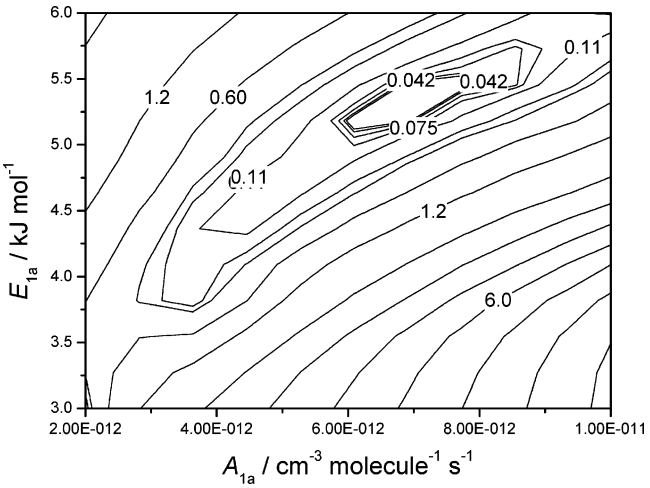

Figure 10. Contour plot of χ^2 from comparing the experimental data with ME fits ($\langle\Delta E\rangle_{down} = 150(T/300\ K)\ cm^{-1}$) for 37 measurements of $k_{1a}(T,P)$ in He, as a function of A_{1a}^{∞} and E_{1a}^{∞}. This surface has a defined minimum at $A_{1a}^{\infty} = 7.1 \times 10^{-12}$ cm^{-3} molecule^{-1} s^{-1} and $E_{1a}^{\infty} = 5.3$ kJ mol^{-1}.

TABLE 7: Extended Troe (Eq 7) Fitting to the Master Equation Output over the Temperature Range 210−373 K

parameter	M	value	units
A_{1a}^{0}	He	$(6.28 \pm .2.28) \times 10^{-29}$	cm^6 molecule^{-2} s^{-1}
E_{1a}^{0}	He	4481 ± 424	J mol^{-1}
$A_{1a}^{¥}$	He	$(8.46 \pm 0.37) \times 10^{-12}$	cm^3 molecule^{-1} s^{-1}
$E_{1a}^{¥}$	He	5257 ± 468	J mol^{-1}
T^*	He	466 ± 33	
P	He	2.69 ± 0.10	
A_{1a}^{0}	N_2	$(1.5 \pm .0.3) \times 10^{-29}$	cm^6 molecule^{-2} s^{-1}
E_{1a}^{0}	N_2	6361 ± 259	J mol^{-1}
$A_{1a}^{¥}$	N_2	8.46×10^{-12} (fixed)	cm^3 molecule^{-1} s^{-1}
$E_{1a}^{¥}$	N_2	5257 (fixed)	J mol^{-1}
T^*	N_2	487 ± 27	
P	N_2	2.50 ± 0.08	

parameters[8] were also determined by fitting to the calculated rate coefficients using a modified Troe representation given by

$$k_{1a}(T) = k_{1a}^{\infty}(T)\frac{k_{1a}^{0}[M]}{k_{1a}^{0}[M] + k_{1a}^{\infty}}F \qquad \text{(E7)}$$

where $\log F = \log F_c/[1 + [\log(k_{1a}^{0}[M]/k_{1a}^{\infty})/N]^2]$, $F_c = \exp(-T/T^*)$, and $N = P - 1.27\log(F_c)$. In order to fit to the calculated rate coefficients, k_{1a}^{0} and k_{1a}^{∞} were assigned Arrhenius forms, that is, $A\exp(-E/RT)$, and the parameters were adjusted using a nonlinear least-squares procedure. Normally a P value of 0.75 is recommended, but much better agreement was obtained with $P = 2.69$ and 2.50 for helium and nitrogen, respectively. The best fit Troe parameters are shown in Table 7. Note that the expression for the high-pressure limit k_{1a}^{∞} differs somewhat from that determined from the ME calculated rate coefficients.

Figure 3 includes the Troe fits and demonstrates the excellent agreement with the results of the ME analysis, to which they were fitted. This procedure, of fitting Troe parameters to data from the optimal ME, has advantages over a straight fit to the experimental data, especially at low pressures, below those accessible experimentally, because the Troe fit is then constrained to a more fundamentally based representation.

Figure 4 shows the room-temperature data for the diluent gases N_2 and SF_6 obtained using CRDS. The data were fitted, using an ME analysis, with k_{1a}^{∞} obtained from the ME fitting to the He data and with $\langle\Delta E\rangle_{down}$ as the only variable parameter.

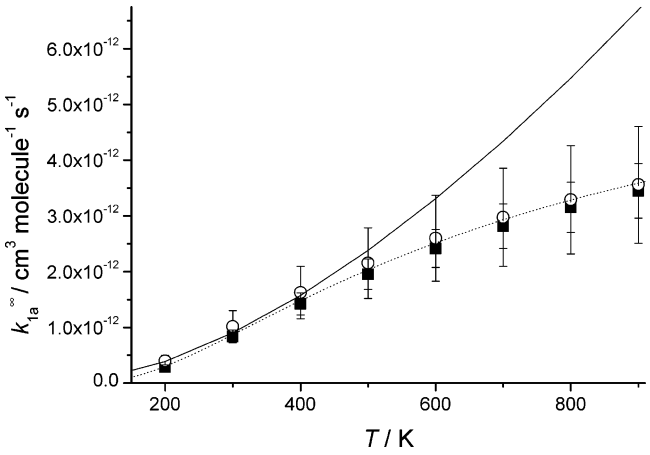

Figure 11. High-pressure rate coefficient for OH ($v = 0$) + C_2H_2, k_{1a}^{∞}, versus T: ○ = this study from analyzing the OH ($v = 1$) data and ■ = this study from ME fitting to the OH ($v = 0$) data. The errors are estimated from Table 6 and the contour plot in Figure 10. The solid line is from the ME analysis of Senosiain et al.[15], and the dotted line is our best fit to all our k_{1a}^{∞}: $A_{1a}^{\infty} = (7.3 \pm 1.3) \times 10^{-12}$ cm^3 molecule^{-1} s^{-1} and $E_{1a}^{\infty} = 5.3 \pm 0.4$ kJ mol^{-1} (errors are 1σ).

A value of 250 cm^{-1} was obtained for N_2. This value was then used, with the temperature dependence for $\langle\Delta E\rangle_{down}$ obtained for He, to generate rate coefficients over a range of temperatures using the ME, which were then fitted using the modified Troe representation, eq 7, and the parameters are reported in Table 7. Figure 4 also shows the data of Sørenson et al.[14] in air, which are somewhat higher than the rate coefficients in N_2 reported here.

The IUPAC evaluation gives $k_{1a}^{0} = 5 \times 10^{-30}(T/K)^{-1.5}$ cm^6 molecule^{-2} s^{-1}, based on a wide range of room-temperature data and the T measurements of Perry et al.,[51] Michael et al.,[10] and Perry and Williamson.[11] They restricted their recommendation to the temperature range 300−800 K. They recommended $k_{1a} = 7.8 \times 10^{-13}$ cm^3 molecule^{-1} s^{-1} in 1 bar of air, a little higher than the value obtained here for 1 bar of N_2 (7.1×10^{-13} cm^3 molecule^{-1} s^{-1}), with $k_{1a}^{\infty} = 1.0 \times 10^{-12}$ cm^3 molecule^{-1} s^{-1}; compare with our 8.6×10^{-13} cm^3 molecule^{-1} s^{-1} (see below) from the combined energy transfer and $v = 0$/ME analysis. Our Troe parameters give $k_{1a}^{\infty} = 8.5 \times 10^{-12}$ cm^3 molecule^{-1} s^{-1}. The IUPAC recommendation is restricted to $T = 298$ K.

General Discussion. The expressions for k_{1a}^{∞} from both the $v = 1,2$ and the $v = 0$ analyses are shown in Figure 11, where they are compared with that given by Senosiain et al.[15] on the basis of a variational transition state/ME model, linked to experimental data. The agreement between all three expressions is remarkably good, especially below 500 K, given the different approaches used. The uncertainty in the expression from $v = 1,2$ is, as noted above, greatest at low T, although the measurements do span the range 195−823 K. The $v = 0$ expression is derived from experimental data that only span the temperature range 210−373 K. For this dataset, the uncertainty in k_{1a}^{∞} is smallest at low T, because the high-pressure limit is most closely approached. The best fit parameters for k_{1a}^{∞}, from the combination of these two datasets, is $A = (7.3 \pm 1.3) \times 10^{-12}$ cm^3 molecule^{-1} s^{-1}and $E = 5.31 \pm 0.43$ kJ mol^{-1} (errors are 1σ).

Senosiain et al.[15] tuned their model using the room-temperature value for k_{1a}^{∞} obtained by Sørenson et al.,[14] which required a lowering of the energy of TS1 (Figure 9a) by 4.4 kJ mol^{-1} to 3.3 kJ mol^{-1}. The temperature-dependent expression they reported for k_{1a}^{∞} (equal to $(1.80 \times 10^{-16}\ (T/K)^{1.34}\exp(-167$

K/T) + 1.00 × 10^{-16} (T/K)$^{1.62}$ exp(−121 K/T)) cm^3 molecule^{-1} s^{-1}) was otherwise determined entirely from variational transition state theory. Figure 11 shows that our low-temperature determinations of k_{1a}^{∞} obtained from the ME fits lie slightly below the calculated values, suggesting that Senosiain et al. may have overestimated the curvature in the Arrhenius plot. They used the data of Michael et al.[10] over the temperature range 228−413 K to parametrize the energy transfer parameter, obtaining $\langle\Delta E\rangle_{down}$ = 160(T/300 K) cm^{-1} for Ar as the bath gas, although the scattered experimental data somewhat compromised this analysis. The ME analysis applied above to the v = 0 data returned $\langle\Delta E\rangle_{down}$ = 150(T/300 K) cm^{-1} for He. The expression for k_{1a}^{∞} of Senosiain et al. also diverges from that from the present analysis at higher temperatures.

The agreement between our data and those of Fulle et al.[7] is less satisfactory. Figure 7 shows a comparison between k_{VET} and their expression for k_{1a}^{∞}. Above 350 K, their values for k_{1a}^{∞} are greater than k_{VET}, which provided IVR is fast compared with dissociation from v = 1,2 is an upper estimate for k_{1a}^{∞}. The ME ILT analysis shows rate constants for the dissociation of the HO−C_2H_2 adduct of ∼5 × 10^9 s^{-1} for v = 1 and ∼5 × 10^{10} s^{-1} for v = 2, at the maximum in the dissociation rate distribution at the low-pressure limit. It would require pathological behavior if IVR were not to compete successfully with dissociation. Silvente et al.[20] obtained rate coefficients for OH + CH_3SCH_3, with $k(v = 2) \sim 2k(v = 1)$, with both significantly less than the high-pressure limit. They ascribed this behavior to slow IVR. This system is quite different because the well depth is much smaller (44−54 kJ mol^{-1} [21,52] versus 130 kJ mol^{-1} for OH + C_2H_2[15]), and the heavier S atom to which OH adds may act to reduce the efficiency of IVR.[53] Such behavior is unlikely in OH + C_2H_2, and the comparison with the analysis of the pressure dependent data for v = 0 and with the results of Senosiain et al. provides convincing validation of the present analysis

The origin of the disagreement with the results of Fulle et al.[7] is not immediately apparent, but may derive from radical reactions resulting from the use 193 nm laser photolysis. The absorption cross section of acetylene at 193.3 nm has been measured as 1.34 × 10^{-20} cm^2 [54] and has a strong vibronic structure, with 193.3 nm lying in a trough between two vibronic bands. Owing to the width of the excimer laser output (±0.5 nm),[55] it is difficult to gauge the effective cross section, but it may be as high as 3.3 × 10^{-20} cm^2. Using the laser power quoted by Fulle et al. (200 mJ) and assuming a 2 cm^2 beam profile (Lambda Physik), we find it can be shown that between 1 and 3% of the acetylene would absorb resulting in significant concentrations of H and C_2H, and also of the long-lived triplet state of C_2H_2. The rate coefficient for OH + C_2H has not been measured but is expected to be reasonably close to gas kinetic. Taking OH + C_2H ∼ 1 × 10^{-10} cm^3 molecule^{-1} s^{-1} and 1% acetylene, we find photolysis gives an effective pseudo-first-order rate coefficient for OH loss of 10^5 s^{-1} at 400 K and [C_2H_2] = 10^{17} molecule cm^{-3}, compared with a measured rate constant at 65 bar of 3 × 10^5 s^{-1}. The increasing discrepancy at higher temperatures could be related to increased absorption by vibrationally excited acetylene.

A further possible source of the higher rate coefficients measured by Fulle et al.[7] could be a contribution from the stabilization of the pre-reaction van der Waals complex, at the high pressures used. Senosiain et al.[15] used a variational analysis that spanned the outer transition state that precedes the van der Waals complex and the inner transition state that precedes the adduct (TS1). They argued that stabilization in the van der Waals well is unlikely at normal pressures, so that the system is conservative across this part of the PES. A crude estimate of the reciprocal lifetime of the pre reaction complex is ∼10^{11} s^{-1}, comparable with the collision frequency at the highest pressures used by Fulle et al. (130 bar). Stabilization in the van der Waals well might increase the rate constant, although this effect would be likely to be greatest at low T, whereas the greatest differences between the present results and those of Fulle et al. occur at high T.

The discrepancy in rate coefficient between OH (v = 1) and OH (v = 2) could arise because the latter contains enough energy (83 kJ mol^{-1}) to surmount the energy barrier for H abstraction, reaction 1b (59 kJ mol^{-1}). This channel lies above the reactant energy for OH (v = 1), which has 43 kJ mol^{-1} of excess vibrational energy. If the difference between OH (v = 1 and 2) were due to this abstraction reaction, it is unlikely that they would have such a similar temperature dependence. In addition, the OH bond is a spectator in the reaction, and so vibrational enhancement of the rate is unlikely. It is also unlikely that the rate of reaction over TS2 would be subject to vibrational enhancement. Figure 9b shows the displacement vectors for the reaction coordinate. They involve angular coordinates rather than the OH stretch. In addition, vibrational enhancement could only occur if the OH vibrational excitation persisted in the adduct HOC_2H_2, that is, if IVR were slow.

6. Conclusions and Summary.

(i) The rate coefficients for the removal of OH (v = 1 and 2) by C_2H_2 has been studied as a function of temperature (195−823 K) using LFP coupled with LIF. The dependence of the rate coefficients on temperature and on the vibrational quantum number demonstrates that there is a significant contribution from what has been termed nonreactive vibrational relaxation, in which the potential energy well of the chemical adduct, HOC_2H_2, is not significantly sampled. The temperature dependence shows, instead, behavior typical of cascade ($\Delta v = -1$) vibrational relaxation influenced by the attractive van der Waals interaction and by the repulsive wall of the interaction potential.

(ii) Analysis of the data using a mechanism that incorporates both nonreactive energy transfer and energy transfer that involves formation of the chemical adduct allows k_{1a}^{∞}, the high-pressure limiting rate coefficient for the formation of the adduct, to be determined to good accuracy over the experimental temperature range.

(iii) OH (v = 0) + C_2H_2 was also investigated over the pressure and temperature ranges 5−500 Torr and 210−373 K, respectively, in a helium bath gas. The data were analyzed using an ME model that was used to fit the Arrhenius parameters for k_{1a}^{∞} and the energy transfer parameter, $\langle\Delta E\rangle_{down}$, to the experimental results. The minimum on the χ^2 hypersurface is well-defined, and the parameters were determined to good accuracy.

(iv) The representations of k_{1a}^{∞} from the two distinct methods agree very well giving the combined Arrhenius parameters A_{1a}^{∞} = (7.3 ± 1.3) × 10^{-12} cm^3 molecule^{-1} s^{-1} and E_{1a}^{∞} = 5.3 ± 0.4 kJ mol^{-1}, where the uncertainties are ±1σ.

(v) Measurements were also made at room temperature for OH (v = 0) in N_2 and SF_6, using CRDS. These measurements were combined with k_{1a}^{∞} to obtain $\langle\Delta E\rangle_{down}$ for N_2.

(vi) The data show good agreement with the IUPAC evaluation at room temperature. They made a recommendation for the temperature dependence of k_{1a}^{∞}. The present data provide a reliable set of data for temperatures appropriate to the upper troposphere. The higher temperature values for k_{1a}^{∞} differ

significantly from those determined by Fulle et al. using high-pressure techniques.

Acknowledgment. We thank NERC (COSMAS (NER/T/S/2002/00039)), the Composition Directorate of the National Centre for Atmospheric Science, and the EU SCOUT (GOCE-2004-505390) programme for funding.

References and Notes

(1) Blake, N. J.; Blake, D. R.; Sive, B. C.; Chen, T. Y.; Rowland, F. S.; Collins, J. E.; Sachse, G. W.; Anderson, B. E. *J. Geophys. Res., [Atmos.]* **1996**, *101*, 24151−24164.

(2) Baulch, D. L.; Bowman, C. T.; Cobos, C. J.; Cox, R. A.; Just, T.; Kerr, J. A.; Pilling, M. J.; Stocker, D.; Troe, J.; Tsang, W.; Walker, R. W.; Warnatz, J. *J. Phys. Chem. Ref. Data* **2005**, *34*, 757−1397.

(3) Glassman, I. *Combustion*, 3rd ed.; London Academic Press: San Diego, CA, 1996.

(4) Lindstedt, R. P.; Skevis, G. *Combust. Sci. Technol.* **1997**, *125*, 73−137.

(5) Woods, I. T.; Haynes, B. S. *Proc. Combust. Inst.* **1994**, *25*, 909−917.

(6) Atkinson, R.; Baulch, D. L.; Cox, R. A.; Hampson, R. F.; Kerr, J. A.; Rossi, M. J.; Troe, J. *J. Phys. Chem. Ref. Data* **1999**, *28*, 191−393.

(7) Fulle, D.; Hamann, H. F.; Hippler, H.; Jansch, C. P. *Ber. Bunsen-Ges.* **1997**, *101*, 1433−1442.

(8) Troe, J. *Ber. Bunsen-Ges.* **1974**, *78*, 478−488.

(9) Schmidt, V.; Zhu, G. Y.; Becker, K. H.; Fink, E. H. *Ber. Bunsen-Ges.* **1985**, *89*, 321−322.

(10) Michael, J. V.; Nava, D. F.; Borkowski, R. P.; Payne, W. A.; Stief, L. J. *J. Chem. Phys.* **1980**, *73*, 6108−6116.

(11) Perry, R. A.; Williamson, D. *Chem. Phys. Lett.* **1982**, *93*, 331−334.

(12) Wahner, A.; Zetzsch, C. *Ber. Bunsen-Ges.* **1985**, *89*, 323−325.

(13) Atkinson, R.; Baulch, D. L.; Cox, R. A.; Crowley, J. N.; Hampson, R. F.; Hynes, R. G.; Jenkin, M. E.; Rossi, M. J.; Troe, J. *Atmos. Chem. Phys.* **2006**, *6*, 3625−4055.

(14) Sorenson, M.; Kaiser, E. W.; Hurley, M. D.; Wallington, T. J.; Nielson, O. J. *Int. J. Chem. Kinet.* **2003**, *35*, 191.

(15) Senosiain, J. P.; Klippenstein, S. J.; Miller, J. A. *J. Phys. Chem. A* **2005**, *109*, 6045−6055.

(16) Jaffer, J. H.; Smith, I. W. M. *Faraday Discuss. Chem. Soc.* **1979**, *67*, 146.

(17) D'Ottone, L.; Bauer, D.; Campuzano-Jost, P.; Fardy, M.; Hynes, A. J. *Faraday Discuss.* **2005**, *130*, 111−123.

(18) Blitz, M. A.; Hughes, K. J.; Pilling, M. J. *J. Phys. Chem. A* **2003**, *107*, 1971−1978.

(19) Smith, I. W. M. *Chem. Soc. Rev.* **1985**, *14*, 141−160.

(20) Silvente, E.; Richter, R. C.; Hynes, A. J. *J. Chem. Soc., Faraday Trans.* **1997**, *93*, 2821−2830.

(21) Barone, S. B.; Turnipseed, A. A.; Ravishankara, A. R. *J. Phys. Chem.* **1996**, *100*, 14694−14702.

(22) O'Keefe, A.; Deacon, D. A. G. *Rev. Sci. Instrum.* **1988**, *59*, 2544−2551.

(23) Okabe, H. *Photochemistry of Small Molecules;* Wiley-Interscience: Chichester, U.K., 1978.

(24) Wollenhaupt, M.; Carl, S. A.; Horowitz, A.; Crowley, J. N. *J. Phys. Chem. A* **2000**, *104*, 2695−2705.

(25) Dai, J. Q. *J. Chem. Phys.* **1997**, *107*, 4934−4942.

(26) Aker, P. M.; Sloan, J. J. *J. Chem. Phys.* **1986**, *85*, 1412−1417.

(27) Rensberger, K. J.; Jeffries, J. B.; Crosley, D. R. *J. Chem. Phys.* **1989**, *90*, 2174−2181.

(28) Blitz, M. A.; Hughes, K. J.; Pilling, M. J.; Robertson, S. H. *J. Phys. Chem. A* **2006**, *110*, 2996−3009.

(29) Effenhauser, C. S.; Felder, P.; Huber, J. R. *Chem. Phys.* **1990**, *142*, 311−320.

(30) Wilson, M. W.; Rothschild, M.; Muller, D. F.; Rhodes, C. K. *J. Chem. Phys.* **1982**, *77*, 1837−1841.

(31) Dillon, T. J. Laser Studies of Radicals of Atmospheric Importance. University of Leeds, 2002.

(32) Cleary, P. A.; Romero, M. T. B.; Blitz, M. A.; Heard, D. E.; Pilling, M. J.; Seakins, P. W.; Wang, L. *Phys. Chem. Chem. Phys.* **2006**, *8*, 5633−5642.

(33) Greenwald, E. E.; North, S. W.; Georgievskii, Y.; Klippenstein, S. J. *J. Phys. Chem. A* **2005**, *109*, 6031−6044.

(34) Davies, J. W.; Green, N. J. B.; Pilling, M. J. *Chem. Phys. Lett.* **1986**, *126*, 373−379.

(35) Robertson, S. H.; Pilling, M. J.; Baulch, D. L.; Green, N. J. B. *J. Phys. Chem.* **1995**, *99*, 13452−13460.

(36) Miller, J. A.; Klippenstein, S. J. *J. Phys. Chem. A* **2003**, *107*, 2680−2692.

(37) Klippenstein, S. J.; Miller, J. A. *J. Phys. Chem. A* **2002**, *106*, 9267−9277.

(38) Sosa, C.; Schlegel, H. B. *J. Am. Chem. Soc.* **1987**, *109*, 4193−4198.

(39) Miller, J. A.; Melius, C. F. A Theoretical Analysis of the Reaction Between Hydroxyl and Acetylene. In *Twenty Second Symposium (International) on Combustion*; The Combustion Institute: Pittsburg, PA, 1988; pp 1031−1039.

(40) Davey, J. B.; Greenslade, M. E.; Marshall, M. D.; Lester, M. I.; Wheeler, M. D. *J. Chem. Phys.* **2004**, *121*, 3009−3018.

(41) Montgomery, J. A., Jr.; Ochterski, J. W.; Petersson, G. A. *J. Chem. Phys.* **1994**, *101*, 5900−5909.

(42) Frisch, M. J.; Trucks, G. W.; Schlegel, H. B.; Scuseria, G. E.; Robb, M. A.; Cheeseman, J. R.; Montgomery, J. A., Jr.; Vreven, T.; Kudin, K. N.; Burant, J. C.; Millam, J. M.; Iyengar, S. S.; Tomasi, J.; Barone, V.; Mennucci, B.; Cossi, M.; Scalmani, G.; Rega, N.; Petersson, G. A.; Nakatsuji, H.; Hada, M.; Ehara, M.; Toyota, K.; Fukuda, R.; Hasegawa, J.; Ishida, M.; Nakajima, T.; Honda, Y.; Kitao, O.; Nakai, H.; Klene, M.; Li, X.; Knox, J. E.; Hratchian, H. P.; Cross, J. B.; Bakken, V.; Adamo, C.; Jaramillo, J.; Gomperts, R.; Stratmann, R. E.; Yazyev, O.; Austin, A. J.; Cammi, R.; Pomelli, C.; Ochterski, J. W.; Ayala, P. Y.; Morokuma, K.; Voth, G. A.; Salvador, P.; Dannenberg, J. J.; Zakrzewski, V. G.; Dapprich, S.; Daniels, A. D.; Strain, M. C.; Farkas, O.; Malick, D. K.; Rabuck, A. D.; Raghavachari, K.; Foresman, J. B.; Ortiz, J. V.; Cui, Q.; Baboul, A. G.; Clifford, S.; Cioslowski, J.; Stefanov, B. B.; Liu, G.; Liashenko, A.; Piskorz, P.; Komaromi, I.; Martin, R. L.; Fox, D. J.; Keith, T.; Al-Laham, M. A.; Peng, C. Y.; Nanayakkara, A.; Challacombe, M.; Gill, P. M. W.; Johnson, B.; Chen, W.; Wong, M. W.; Gonzalez, C.; Pople, J. A. *Gaussian 03*, revision B.03; Gaussian, Inc.: Pittsburg, PA, 2003.

(43) Luque, J.; Crosley, D. R. LIFBASE: Database and Spectral Simulation Program, 1.5 ed.; SRI International Report MP 99−009, 1999.

(44) Shin, H. K. *J. Am. Chem. Soc.* **1968**, *90*, 3029.

(45) Chance, E. M.; Curtis, A. R.; Jones, I. P.; Kirby, C. R. *FACSIMILE: a computer program for flow and chemistry simulation, and general initial value problems*; Department of Biochemistry, University College: London, U.K., 1977.

(46) Lambert, J. D. *Vibrational and Rotational Relaxation in Gases*; Clarendon Press: Oxford, U.K., 1978.

(47) Shin, H. K. *Chem. Phys. Lett.* **1971**, *10*, 81.

(48) Shin, H. K. *J. Phys. Chem.* **1971**, *75*, 1079.

(49) Dodd, J. A.; Lipson, S. J.; Blumberg, W. A. M. *J. Chem. Phys.* **1991**, *95*, 5752−5762.

(50) Tao, F.-M.; Klemperer, W. *J. Chem. Phys.* **1995**, *103*, 950−956.

(51) Perry, R. A.; Atkinson, R.; Pitts, J. N., Jr. *Chem. Phys.* **1977**, *67*, 5577.

(52) Hynes, A. J.; Stoker, R. B.; Pounds, A. J.; McKay, T.; Bradshaw, J. D.; Nicovich, J. M.; Wine, P. H. **1995**, *99*, 16967−16975.

(53) Lopez, V.; Marcus, R. A. *Chem. Phys. Lett.* **1982**, *93*, 232−234.

(54) Seki, K.; Okabe, H. *J. Phys. Chem.* **1993**, *97*, 5284−5290.

(55) Hoffman, J. M.; Hays, A. K.; Tisone, G. C. *Appl. Phys.* **1976**, *28*, 538.

(56) Herzberg, G. *Molecular Spectra and Molecular Structure, III, Electronic Spectra of Polyatomic Molecules*; Van Nostrand Reinhold Co.: New York, 1966.

(57) Huber, K. P.; Herzberg, G. *Molecular Spectra and Molecular Structure, IV, Constants of Diatomic Molecules*; Van Nostrand Reinhold Co.: New York, 1979.